

Structural, optical, electrical properties and FTIR studies of fluorine doped SnO_2 films deposited by spray pyrolysis

B. Zhang · Y. Tian · J. X. Zhang · W. Cai

Received: 20 July 2010/Accepted: 20 October 2010/Published online: 11 November 2010
© Springer Science+Business Media, LLC 2010

Abstract Thin films of $\text{SnO}_2:\text{F}$ were prepared by ultrasonic spray pyrolysis method. The effect of fluorine concentration on the structural, optical, and electrical properties of $\text{SnO}_2:\text{F}$ films was investigated. The X-ray diffraction results showed the preferred growth along (110). FTIR was employed to study the defects in SnO_2 lattice. The evidence of oxygen vacancy and substitution of fluorine for oxygen in FTIR were investigated. It was found that at low doping levels, fluorine ions preferred to replace the oxygen in the lattice. While beyond a certain doping level, fluorine ions started to occupy interstitial site, which had a negative effect on carrier concentration that, in turn, affected the infrared reflectivity of $\text{SnO}_2:\text{F}$ films. The increased disorder of SnO_2 at high doping levels was also shown by FTIR. The discussion of carrier scattering suggested that ionized impurity and/or neutral impurity scattering were the dominant scattering mechanisms in $\text{SnO}_2:\text{F}$ films.

Introduction

Tin oxide (SnO_2) has been recognized as an attractive material due to its excellent optical properties, chemical durability, and transparent conductivity. Recent years have witnessed its extensive using in solar cells, liquid crystal

displays, low emission glass and heat mirrors [1–3]. However, the undoped stoichiometric SnO_2 has low optical and electrical performance because of its low intrinsic carrier density and mobility. Doping with antimony (Sb), indium (In), and fluorine (F) is used to improve its optical properties and conductivity [4–6]. Among these dopants, fluorine has been shown to be effective and used in many commercial applications.

Thin films of SnO_2 can be prepared by many techniques, such as chemical vapor deposition [7], sputtering [8], sol–gel [9], reactive evaporation [10], pulsed laser ablation [11], screen printing technique [12], and spray pyrolysis [13]. Among these, spray pyrolysis is the most convenient method because of its simplicity, low cost, easy to add doping materials, and the possibility of varying the film properties by changing composition of starting solution. Otherwise, this method is promising for high rate and mass production capability of uniform large area coatings in industry.

A thorough survey of literature reveals that most research works focus on the electrical properties of $\text{SnO}_2:\text{F}$ films, but very little information on the role of fluorine and their effects on the film structure. In this paper, we used FTIR to investigate the role of fluorine in $\text{SnO}_2:\text{F}$ films. The relationship between the features in FTIR, film structure and carrier concentration was described. The experimental evidence of oxygen vacancy and substitution of fluorine for oxygen was suggested by FTIR. The varied film structural, optical, and electrical properties with different fluorine concentrations were also shown in this paper.

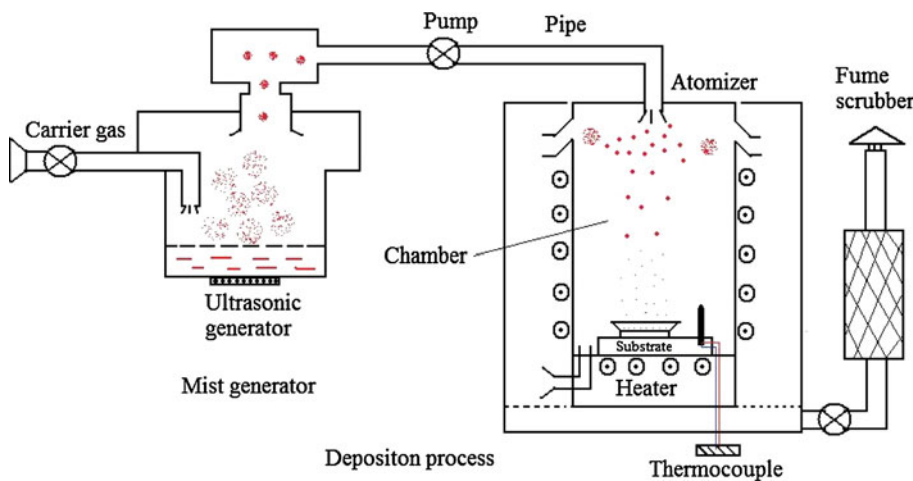
Materials and methods

An aqueous solution of high pure tin chloride ($\text{SnCl}_2 \cdot 2\text{H}_2\text{O}$) was used as starting solution. The concentration of the

B. Zhang · J. X. Zhang · W. Cai
School of Materials Science and Engineering, Harbin Institute of Technology, Harbin 150001, People's Republic of China

B. Zhang · Y. Tian · J. X. Zhang (✉)
School of Materials Science and Engineering, Shandong University, 73 Jingshi Road, Jinan 250061, Shandong Province, People's Republic of China
e-mail: jianxin@sdu.edu.cn

Fig. 1 The setup of ultrasonic spray pyrolysis equipment



solution was 0.1 mol/L. A small amount of concentrated hydrochloric acid (HCl) was added to prevent hydrolysis. Fluorine doping was achieved by adding ammonium fluoride (NH_4F) to the solution, fixed at 0, 5, 10, 15, 20, 25 wt%.

The $\text{SnO}_2:\text{F}$ films were prepared by an ultrasonic spray pyrolysis coating setup. Its schematic diagram was as Fig. 1. The substrates were soda-lime glass and KBr (for FTIR). The deposition temperature was 350 °C. The atomization rate was 3–4 mL/min and the spray process was not continuous with an intermittence to keep the temperature of substrates. The samples were naturally cooled down after deposition.

The crystalline characteristic of $\text{SnO}_2:\text{F}$ films was studied by XRD (RINT-2200, Rigaku) using $\text{Cu K}\alpha$ radiation. The morphology and composition of the films was obtained by scanning electron microscope (SEM) (JSM6610lv, JEOL) with energy dispersive spectrometer (OXFORD). A UV-Vis-Nir double-beam spectrophotometer (Lambda950, PerkinElmer) was used to measure the optical transmittance and reflectance of the films in wavelength of 200–3000 nm. The carrier concentration and Hall mobility was obtained by a Hall Effect measurement (HMS3000, Ecopia) in Van Der Pauw configuration at room temperature.

Results and discussion

Structural studies

The X-ray diffraction patterns of $\text{SnO}_2:\text{F}$ films are shown in Fig. 2. All the films are found to be tetragonal rutile structure and a polycrystalline nature with preferred orientation along (110). Other peaks (200), (101), (211), (220), (310), and (301) are also observed, but with low intensities. No feature of fluoride has been observed in the patterns, which is possibly due to the resolution of XRD.

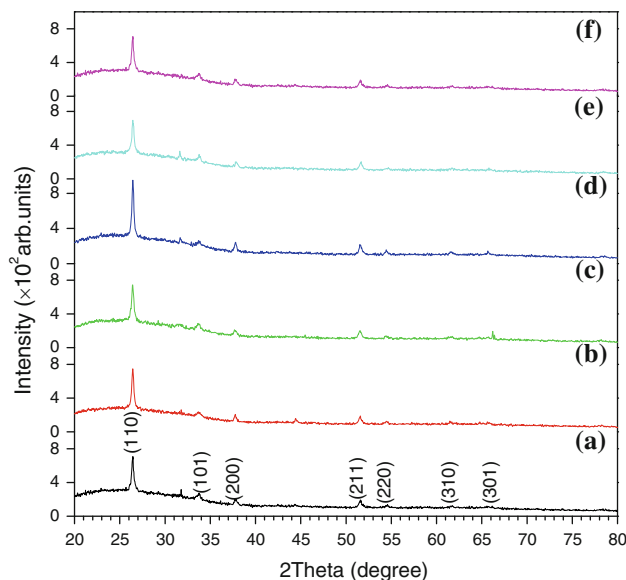


Fig. 2 The X-ray diffraction patterns of $\text{SnO}_2:\text{F}$ films: (a) 0 wt%, (b) 5 wt%, (c) 10 wt%, (d) 15 wt%, (e) 20 wt%, (f) 25 wt% of NH_4F in the spray solution

The actual fluorine content in the film is shown in Table 1, which is obtained by the EDX.

The preferred orientation of $\text{SnO}_2:\text{F}$ films can be ascribed to the difference in preparation. Many parameters have been found to be effective on the film growth, such as tin precursor [14], additive in solution [15], and film thickness [16]. Goyal et al. [17] have reported that at low doping concentration, the SnO_2 film grows along (110), and it changes gradually to (200) with an increase of fluorine concentration. It also has been reported that the film prepared from SnCl_2 contains a disordered growth [18]. In the present case, the preferred growth along (110) remains predominant irrespective of fluorine doping levels. The reason can be sought from the low deposition temperature in preparation. It is well confirmed by report [19], in which

Table 1 Data for scattering mechanism analysis of $\text{SnO}_2:\text{F}$ films

Sample (No.)	Fluorine content (F/Sn at.%)	Crystallite size (Å)	Mean free path (Å)	Mobility ($\text{cm}^2 \text{V}^{-1} \text{s}^{-1}$)
0 wt%	None	318	9.5	8
5 wt%	Undetectable	547	20.7	6
10 wt%	0.24	1066	11.1	3
15 wt%	0.37	1279	9.4	2.4
20 wt%	0.50	961	7.5	2
25 wt%	0.61	685	5.5	1.6

Masayuki et al. have prepared $\text{SnO}_2:\text{F}$ films at various substrate temperatures with the butylene solution, and their results showed the highest crystallinity along (110) at 340 °C, which changed to (200) at 480 °C.

To obtain more details of defects in $\text{SnO}_2:\text{F}$ films FTIR is employed. Selected region of the recorded spectrum for $\text{SnO}_2:\text{F}$ films is shown as Fig. 3. The main IR features of SnO_2 at 468 and 619 cm⁻¹ are assigned to O–Sn–O and Sn–O stretching vibrations, respectively [4]. Two interesting features can be identified: one is the weak feature of O–Sn–O vibration in the undoped SnO_2 film, which goes with the presence of vibration at 644 cm⁻¹. This vibration becomes weakened and disappears as the increase of fluorine concentration; the other characteristic is the presence of Sn–F(α -SnF₂) feature at high doping levels, which causes the splitting of O–Sn–O feature. It is also found that the Sn–O stretching vibration frequency shows an red shift from 619 cm⁻¹ to 605 cm⁻¹ after the doping level of 15 wt%.

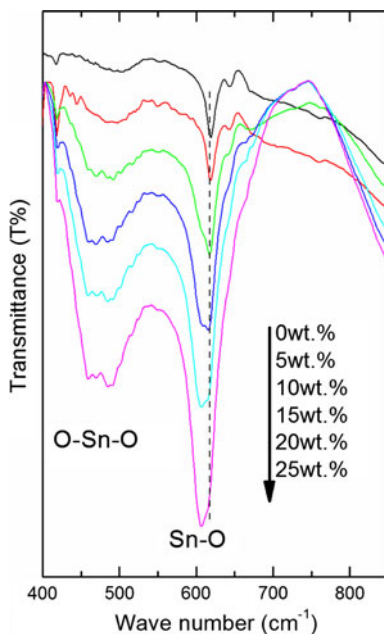
In order to gain a better insight into oxygen vacancy (V_O^{2+}) and substitution of fluorine for oxygen (F_O^{1+}), we

have systematically studied the features in FTIR. There are two lattice sites for oxygen ($u,u,0;0.5 + u,0.5-u,0.5$) in SnO_2 lattice, which correspond to the oxygen in the group of O–Sn–O and Sn–O. So, the vibrational features of O–Sn–O and Sn–O can reflect the defects in SnO_2 lattice, especially on the oxygen site. For V_O^{2+} , it is easy to occur on the group of O–Sn–O because of the different bond length (O–Sn–O: 2.597 Å; Sn–O: 2.053 Å). The presence of V_O^{2+} can deform the O–Sn–O group to O–Sn– V_O , which is seemingly as a deformed Sn–O group. It is that the repulsive force between Sn^{4+} and V_O^{2+} ($\text{O}^{2-}-\text{Sn}^{4+}-\text{V}_\text{O}^{2+}$) has a compression effect on the deformed Sn–O. The compressed Sn–O bond shows an increased vibration frequency at 644 cm⁻¹ in FTIR according to the harmonic oscillator model. Thus, the feature at 644 cm⁻¹ can be identified as the indication of V_O^{2+} in SnO_2 lattice. This feature weakens and disappears as fluorine concentration increases, which further corroborates our hypothesis of V_O^{2+} in SnO_2 lattice.

When fluorine is introduced into the SnO_2 lattice, the fluorine has been supposed to substitute oxygen as the following reasons [20]: the similar ionic size (F^- : 0.133 nm, O^{2-} : 0.132 nm), the comparable bond energy with Sn (Sn–O bond ~31.05 D°/kJ mol⁻¹, Sn–F bond ~26.75 D°/kJ mol⁻¹), and Coulomb forces that bind the lattice together are reduced, since the charge on the F^- is only half of the charge on the O^{2-} . Thus, geometrically the lattice is nearly unable to distinguish between F^- and O^{2-} . In the present case, the presence of SnF₂ feature at 484 cm⁻¹ in FTIR provides the experimental evidence for this substitution. In the substitution, each F^- substitutes an O^{2-} in SnO_2 , and the substituted O^{2-} provides free electrons. However, there is a solubility limit of fluorine atoms in SnO_2 lattice beyond which the excess fluorine atoms could not occupy the proper lattice site, but to occupy the interstitial site in SnO_2 lattice. The interstitial fluorine increases the disorder of the lattice remarkably, which results in the red shift of Sn–O vibration frequency in FTIR.

Morphological studies

The SEM images recorded on the surfaces of SnO_2 films are shown in Fig. 4. The characteristic of the morphology

**Fig. 3** The FTIR spectrum of $\text{SnO}_2:\text{F}$ films

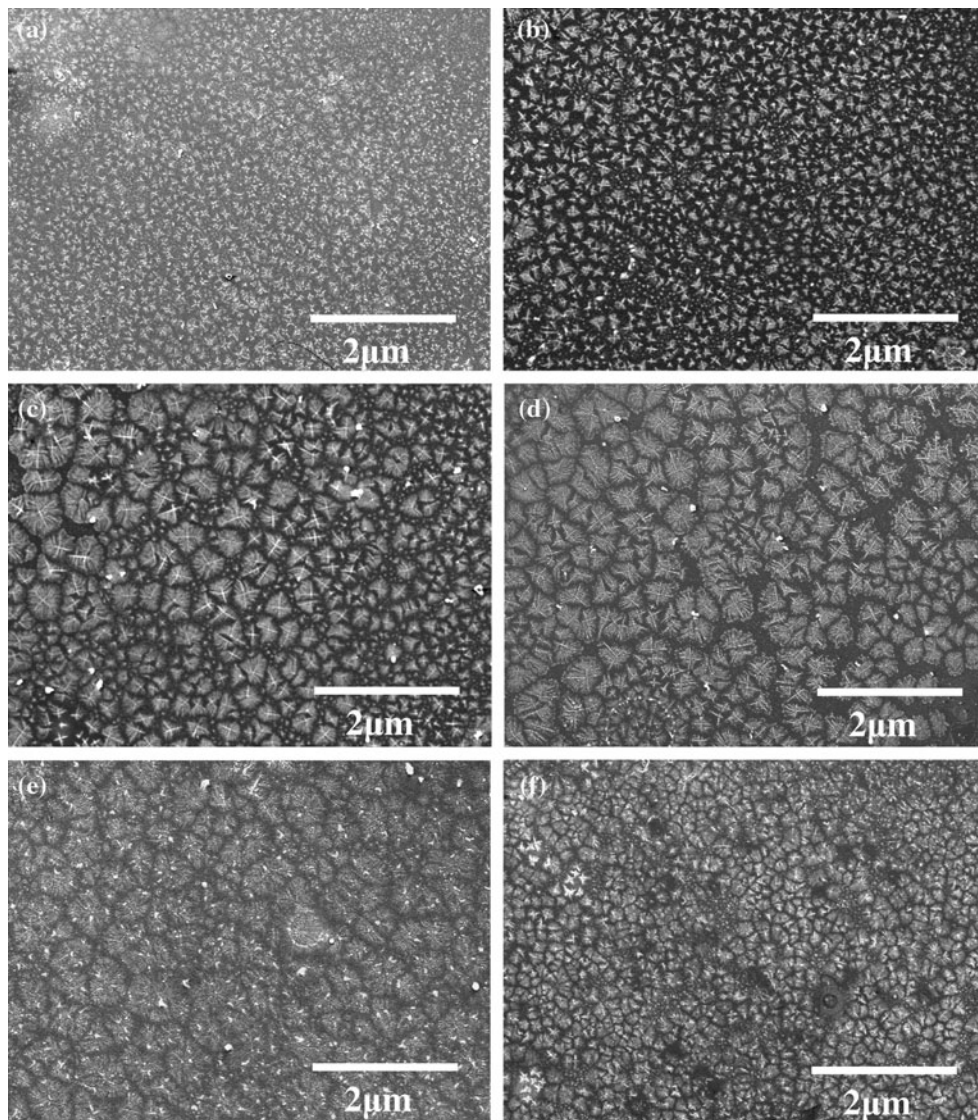


Fig. 4 The morphology of SnO₂:F films: **a** 0 wt%, **b** 5 wt%, **c** 10 wt%, **d** 15 wt%, **e** 20 wt%, **f** 25 wt% of NH₄F in the spray solution

is the tetragonous-shaped grains. The surfaces are found to be uniform and homogeneous, and show the similar morphologies irrespective of fluorine concentration. This consistency in morphology goes well with the same orientation of the films. The large grains can be found from the films with doping of 10, 15, and 20 wt%.

The grain shape has a close connection with growth orientation. Elangovan et al. [20] have reported that the needle-shaped grains show a preferred orientation along (200), whereas the rectangular- and cuboidal-shaped grains orient along (301) and (211), respectively. The tetragonous-shaped grains in our case should correspond to the orientation along (110). Ravichandran et al. [21] have obtained the similar grain shape in their report, in which the films were deposited by perfume atomizer method also have an orientation along (110).

Optical studies

The transmittance and reflectance spectra of SnO₂:F films in wavelength of 200–3000 nm are shown in Fig. 5. The transmittance values are almost equal for various fluorine concentrations, and the undoped SnO₂ film shows a transmittance value as high as 83%. The color of the SnO₂ film is milk white and it turns colorless at the doping of 15 wt%. A light trace of dark color is seen in the film with doping of 25 wt%. Kojima et al. [22] have studied the blackening of the SnO₂ films, reported that the blackening must result from light absorption in the films. The typical reflection spectrum of SnO₂:F films is described as Fig. 5b. The reflectivity is almost a constant whereas it shows an increase after the wavelength of 1500 nm. The reflectivity properties of SnO₂:F films show an increase till doping of

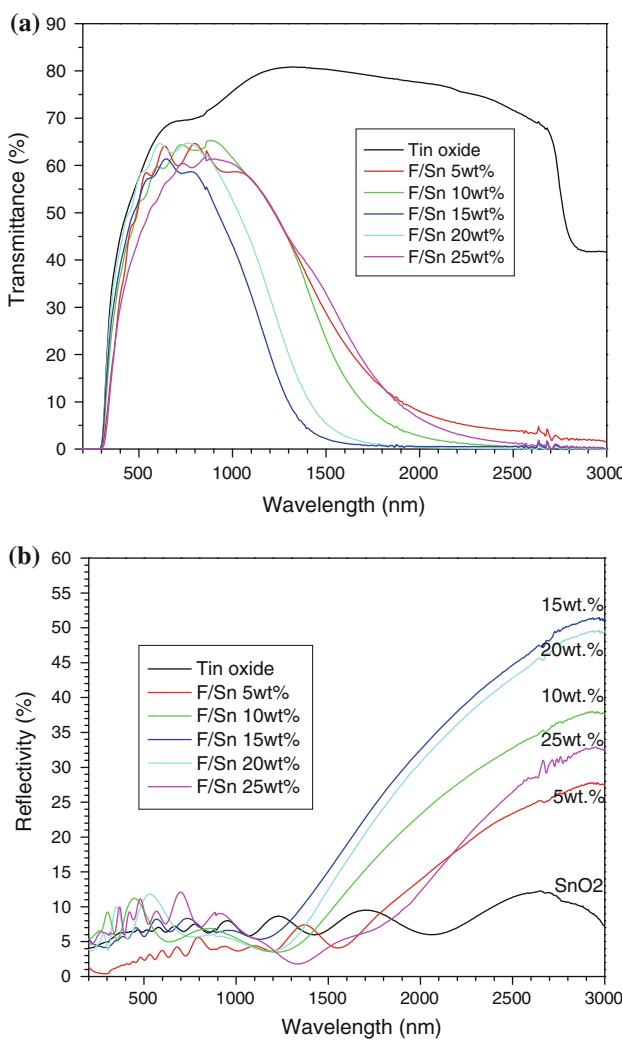


Fig. 5 The optical transmittance and reflectance of f $\text{SnO}_2:\text{F}$ films: **a** Transmittance, **b** reflectance

15 wt% afterwards decrease for the further rise of fluorine concentration.

The optical characteristic of $\text{SnO}_2:\text{F}$ films is that they have a transmission window between wavelength 0.4 and 1.5 μm . At wavelengths shorter than 0.4 μm , absorption occurs due to the fundamental band gap, and thus light cannot be transmitted due to a quantum phenomenon [23]. The short-wavelength cutoff corresponds to the fundamental band gap energy of the materials; at longer wavelengths, reflection occurs because of the plasma edge, and light cannot be transmitted due to a classical phenomenon. The long-wavelength edge corresponds to the free-carrier plasma resonance frequency ω_p . Based on Maxwell's equations and the Drude theory of free electrons, the quantity ω_p can be derived as Eq. 1 [24]

$$\omega_p = \left(\frac{ne^2}{\epsilon_0 \epsilon_\infty m_c^*} \right), \quad (1)$$

where n is the carrier concentration, e is the electronic charge, ϵ_0 is the permittivity of free space, ϵ_∞ is the high-frequency permittivity, and m_c^* is the conductivity effective mass. At high frequencies ($\omega > \omega_p$), the SnO_2 film behaves like a perfect dielectric, whereas at sufficiently low frequencies ($\omega < \omega_p$), at which both refractive index and extinction coefficient are large, the material has near-unity reflectance as expected from the Fresnel expression for the reflection coefficient. From Eq. 1, it is clear that the carrier concentration in material plays the key role for the films reflectivity.

Electronic studies

The carrier concentration and Hall mobility as a function of fluorine concentration is described as Fig. 6. The carrier concentration shows an increase till the doping of 15 wt%, and then decreases for the further rise of fluorine concentration. The varied carrier concentrations can ascribe to the defects in film structure. It is that at low doping levels, the substitution of fluorine for oxygen is the main defect in $\text{SnO}_2:\text{F}$ films. In the substituent, each F^- substitutes an O^{2-} in the lattice and the substituted O^{2-} provides more free electrons, which has an active effect on the free carrier initially. But beyond a certain doping level, there are more fluorine atoms than the solution limit of fluorine in SnO_2 lattice, and the excess fluorine atoms could not occupy proper site to provide electrons, but to fill the interstitial site to form interstitial fluorine. The interstitial fluorine is the defect at high doping levels, which can trap free electrons and result in the decrease of carrier concentration.

The mobility of $\text{SnO}_2:\text{F}$ films shows a continuous decrease as the increasing of fluorine concentration. The

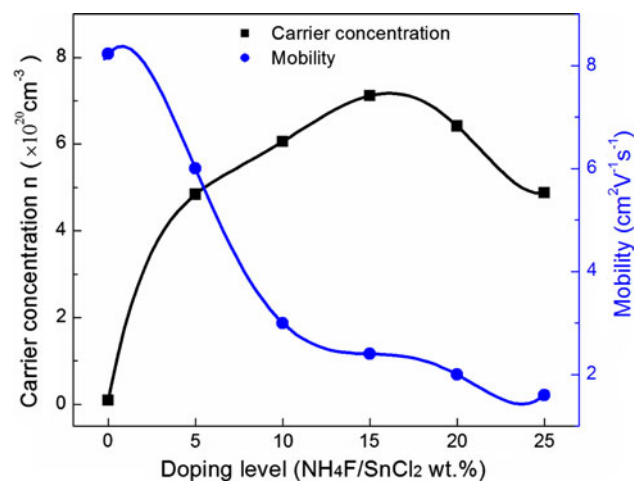


Fig. 6 The variation of carrier concentration and Hall mobility of $\text{SnO}_2:\text{F}$ films

actual value of mobility is determined by the interaction between the various scattering centers and free carriers. In the films prepared by spray pyrolysis method, an ideal lattice cannot be expected. Hence, the scattering of electrons by the thermal vibration of the lattice atoms can be omitted in the case [25]. Thangaraju [26] has verified grain boundary and impurity ion scattering as possible dominant scattering mechanism in the films. The condition of grain boundary scattering to be dominant is the mean free path values should be comparable to crystallite size. In the case, we have calculated the mean free path according to the high degeneracy model. The calculated data of mean free path and crystallite size derived from XRD are shown in Table 1. As can be seen, the mean free path values are considerable shorter than grain size, hence scattering due to grain boundary is not the major factor. The ionized impurity and/or neutral impurity scattering are the dominant scattering mechanisms.

Conclusion

The $\text{SnO}_2:\text{F}$ films have been deposited by spray pyrolysis method. The films show an orientation along (110), which corresponds to the morphology of tetragonus-shaped grains. The FTIR studies provide the experimental evidence of substitution of fluorine for oxygen and oxygen vacancy. The increased disorder of SnO_2 lattice is also revealed by the FTIR. The $\text{SnO}_2:\text{F}$ film with doping of 15 wt% shows optimal optical and electrical properties, at which the electrical conductivity is as high as $2.5 \times 10^3 \text{ S m}^{-1}$. The ionized impurity and/or neutral impurity scattering are the dominant scattering mechanisms.

References

1. Liang HF, Gordon RG (2007) J Mater Sci 42:6388. doi: [10.1007/s10853-006-1255-5](https://doi.org/10.1007/s10853-006-1255-5)

2. Moholkar AV, Pawar SM, Rajpure KY, Bhosale CH, Kim JH (2009) Appl Surf Sci 23:9358
3. Anwar M, Ghauri IM, Siddiqi SA (2008) J Mater Sci 43:6049. doi: [10.1007/s10853-008-2959-5](https://doi.org/10.1007/s10853-008-2959-5)
4. Kuantama E, Han DW, Sung YM, Song JE, Han CH (2009) Thin Solid Films 517:4211
5. Schaefer C, Brauer G, Szczyrbowski J (1997) Surf Coat Technol 93:37
6. Ait Aouaj M, Diaz R, Belayachi A, Rueda F, Abd-lefdil M (2009) Mater Res Bull 44:1458
7. Brown JR, Haycock PW, Smith LM, Jones AC, Williams EW (2000) Sens Actuators B 63:109
8. Boycheva S, Sytchkova AK, Grilli ML, Piegari A (2007) Thin Solid Films 515:8469
9. Banerjee AN, Kundoo S, Saha P, Chattopadhyay KK (2003) J Sol-Gel Sci Technol 28:105
10. Chen W, Ghosh D, Chen SW (2008) J Mater Sci 43:5291. doi: [10.1007/s10853-008-2792-x](https://doi.org/10.1007/s10853-008-2792-x)
11. Kim JH, Jeon KA, Kim GH, Lee SY (2006) Appl Surf Sci 52:4834
12. Berry JJ, Ginley DS, Burrows PE (2008) Appl Phys Lett 92:193304
13. Oshima M, Yoshino K (2010) J Electron Mater 39:816
14. Elangovan E, Ramesh K, Ramamurthi K (2004) Solid State Commun 130:523
15. Smith A, Laurent JM, Smith DS, Bonnet JP, Clemente RR (1995) Thin Solid Films 266:20
16. Elangovan E, Singh MP, Ramamurthi K (2004) Mater Sci Eng B 113:143
17. Goyal DJ, Agashe C, Marathe BR, Takwale MG, Bhinde VG (1993) J Appl Phys 73:7520
18. Gorodillo G, Moreno LC, de la Cruz W, Teheran P (1994) Thin Solid Films 252:61
19. Okuya M, Kaneko S, Hiroshima K, Yagi I, Murakami K (2001) J Eur Ceram Soc 21:2099
20. Elangovan E, Ramamurthi K (2005) Appl Surf Sci 249:183
21. Ravichandran K, Philominathan P (2008) Mater Lett 62:2980
22. Kojima M, Kato H, Gatto M (1993) Philos Mag B 68:215
23. Hamberg I, Hjorberg A, Granqvist CG (1982) Appl Phys Lett 40:362
24. Coutts TJ, Young DL, Li XN (2000) MRS Bull: 58–66
25. Elich JJPh, Boslooper EC, Haitjema H (1989) Thin Solid Films (Electronics and Optics) 177:17
26. Thangaraju B (2002) Thin Solid Films 402:71